Hindawi
Advances in Materials Science and Engineering
Volume 2022, Article ID 9542258, 13 pages
https://doi.org/10.1155/2022/9542258

Research Article

The Effect of Organic and Inorganic Modifiers on the Physical Properties of Granite Residual Soil

Bingxiang Yuan, Weijie Chen, Jin Zhao, Fei Yang, Qingzi Luo, and Tianying Chen

School of Civil and Transportation Engineering, Guangdong University of Technology, Guangzhou 510006, China

Correspondence should be addressed to Fei Yang; 1875104541@qq.com

Received 28 January 2022; Accepted 18 April 2022; Published 30 April 2022

Academic Editor: Qian Chen

As a kind of highly weathered special soil in South China, granite residual soils (GRS) feature high strength and high void ratio in a dry environment, so they tend to disintegrate in water and cause geological disasters including collapse. Therefore, modifying GRS for higher strength has become a hot spot. Glass fiber reinforced soils boast fewer cracks, higher energy absorption, and residual strength. This study aims to analyze the reinforcement effect of glass fibers on GRS with inorganic and organic solutions and its environmental feasibility. The inorganic solution contains silicon ion and sodium ion at the ratio of 1 : 4 (hereinafter referred to as Si : Na = 1 : 4 solutions), and the organic one is a modified polyvinyl alcohol solution (hereinafter referred to as SH solution). The reinforced samples were subjected to plate and impact load tests, SEM, and XRD analysis to investigate their mechanical properties, microcharacteristics, and the components produced. Results indicate that the reinforcement effect of glass fibers on GRS under Si : Na = 1 : 4 solutions was better than that of SH solutions. After being reinforced by Si : Na = 1 : 4 solutions, the samples reached maximum impact resistance. SEM results show that glass fibers bond more soil and form an integral structure; thereby the strength was improved as glass fibers share external impact load. XRD results show that geopolymer and alkali-activated materials and potassium feldspar were formed. Geopolymer and alkali-activated materials are pollution-free, inorganic polymers featuring viscosity and high compressive strength. Potassium feldspar is an aluminosilicate mineral with high strength and stable chemical properties, which can adhere to more granules and form a stronger whole structure with geopolymers playing a role. Therefore, it is feasible to reuse these soils sustainably by reinforcing them with glass fibers and the best Si : Na = 1 : 4 solutions. This study finds a new direction for recycling and reusing construction waste, GRS.

1. Introduction

As China's economy takes off in recent years, domestic infrastructure projects expand at a frenetic pace, some of which are subways, deep foundation pits, and other urban underground space construction projects. Accompanied with that, concerns over construction waste soil are picking up. It is estimated that China excavated more than 2 million tons of construction waste in 2019 alone [1], most of which in South China is granite residual soil (GRS). Owing to its porosity and water absorption, collapse and erosion occur under the influence of wetting-drying cycles, so the soil is usually excavated and carried off as waste in engineering [2]. However, in South China, the thickness of GRS often reaches a depth of over 10–20 meters or even 30 meters. In practice, a huge stack area is required for excavation and a large amount of dust will be generated during transportation, resulting in a huge expense and environmental pollution [3, 4]. Widely distributed in South China, GRS is produced under specific geographical conditions, climate, and geological environments. Since it has special composition and structure, it is also called a regional special soil [5]. The physical and chemical weathering made its distinctive structure with heterogeneity and anisotropy and its unique engineering geomechanical characteristics [6–8]. The majority of South China is characterized by the subtropical and tropical monsoon climate. Affected by the dry-wet cycle climate in this region, GRS is easy to soften and disintegrate in water and, once disturbed, prone to induce geological disasters including landslides and collapse (Figure 1), which will

Figure 1: Granite residual soil in Youxi, Fujian province.

interrupt the construction of slopes and subgrade [9–11]. Currently, most of the granite residual soil is treated by landfills. The profound reason for the waste of GRS is its special structure performance, to be more specific, its high porosity, which makes it unstable and easy to collapse in water [12–14]. However, as the concept of sustainability and environmental protection takes root in people, modifying and reusing GRS has become a heated topic in recent years and attracted the attention of many scholars [15–17].

For instance, a reinforcement system for kaolin was formed by using industrial waste, steel slag, and slag as raw materials, and adding active magnesium oxide and calcium oxide. Results show that the overall skeleton structure formed by the reinforcement system enjoys greater strength [18, 19]. In another research, the properties of modified concrete were improved by using kaolinite from waste soil as raw material and adding concrete [20–22]. All the above methods improve the mechanical properties and water stability of granite residual soil. However, these methods are difficult to apply widely because they cannot improve soil's mechanical properties and water stability while being environmentally friendly and achieving lower carbon emissions. Therefore, to improve GRS, several scholars have made in-depth research. Some studies found that GRS' porosity and hydrophilicity are the main reason for its poor mechanical performance [7, 23, 24]. For hydrophilicity, some scholars conducted disintegration resistance tests and found that GRS is very easy to disintegrate in water, resulting in the loss of strength [25–27]. The hydrophilicity of GRS is related to kaolinite clay, its main mineral component. The octahedral surface containing hydroxyl in the kaolinite crystal structure is prone to form a strong hydrogen bond with water, so kaolinite exhibits strong hydrophilicity, which makes GRS prone to collapse in water [28–30]. At the same time, some studies have shown that some properties of transparent soil reinforcement are similar to those of granite residual soil [8, 19, 31, 32]. GRS also contains a large amount of silica, which can affect the strength of the soil [30, 33–35].

To deal with GRS' special structure and the poor water stability in an environment-friendly way, some scholars studied changing the chemical composition of soil with inorganic and organic solutions [36–38]. By changing the content of ions in the soil, it was found that the proportion and concentration of ions will affect the strength of granite residual soil [39–41]. The organic SH solution can improve the strength and bearing capacity of GRS by changing the content of hydroxyl in it [42–44]. Different lengths of polypropylene fibers were used to reinforce soft soil to study the effect of fibers on soft soil reinforcement [45–47]. Results show that their shear strength rises as the content and length of the fibers increase. Fiber reinforcement also results in a reduction of the compressibility of the soft clay at consecutive consolidation and shear stages. Meanwhile, some studies have shown that adding glass fibers to GRS with the organic solution can reduce cracks and improve water stability and bearing capacity [42, 48–52].

From the above studies, many scholars have studied reinforcing GRS with fibers, organic solutions, or chemical treatments and verified the reinforcement effect by static load tests. But there is no sufficient in-depth research on the microscopic mechanism of different green chemical solutions and organic modifiers on GRS, leaving their mechanism unclear. Therefore, the purpose of this study is to compare the effects of different modifiers (SH solution and $Si:Na = 1:4$ solutions) on reinforcement and the impact resistance of GRS, to analyze the mechanism of different modifiers, and to investigate their influences on the chemical and physical properties of the soil by SEM and XRD.

2. Experimental Materials and Methods

2.1. Raw Materials. Granite Residual Soils (GRS) are characterized by strong structural connections and high strength. They are produced under specific climates, landforms, and geological environments, featuring special composition and structural characteristics. The granite residual soils used in this experiment came from the Guangzhou area, often comprised of mottled reddish-brown, yellowish-brown, gray-white colors, mainly constituted of cohesive soil and partly cobbly cohesive soil. Figure 2(a) shows the granite residual soil used in the experiment, and its basic soil engineering properties are reported in Table 1. Figure 2(b) shows the A.P. sodium hydroxide used in the experiment. Sodium hydroxide analytical pure is white uniform granules with a density of 1.09 g/cm^3 and a relative molecular mass of 40, soluble, and transparent after dissolving in water. Figure 2(c) shows the A.P. sodium silicate used in the experiment. Sodium silicate is white uniform granules with

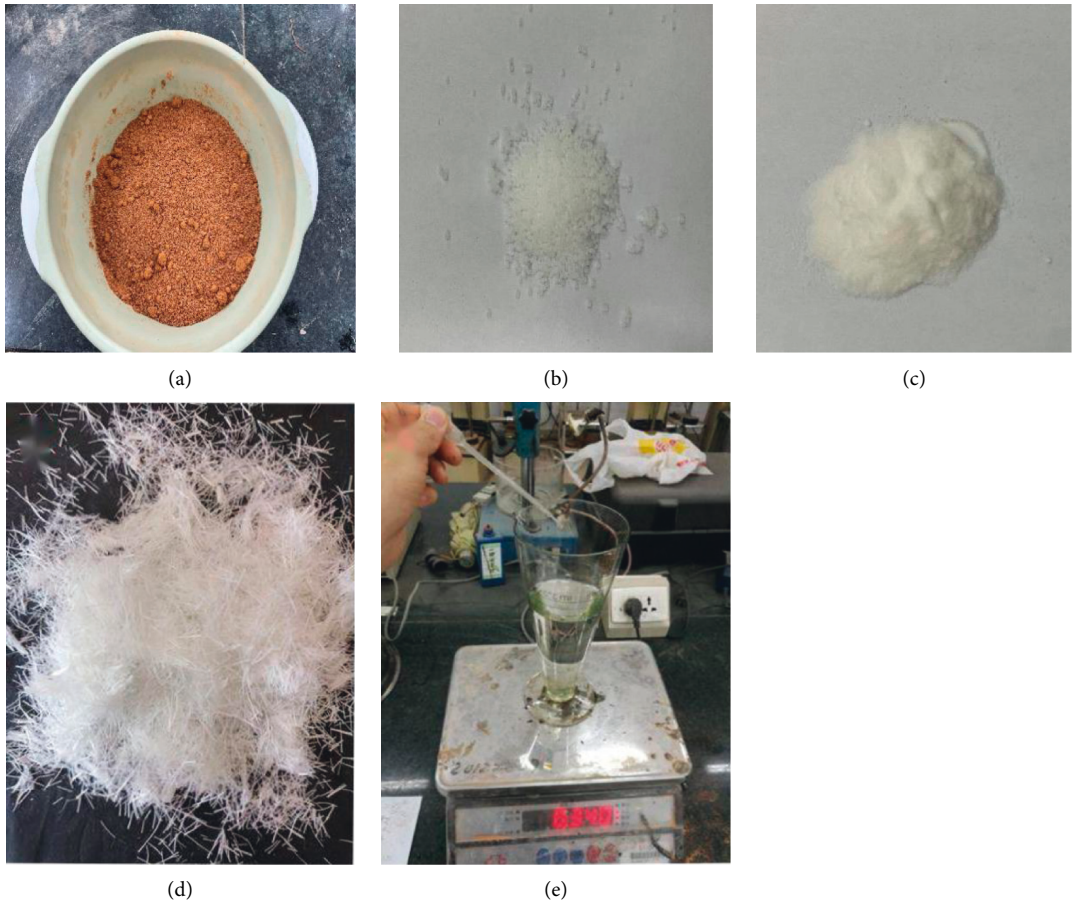

Figure 2: Material diagram: (a) granite residual soil, (b) sodium hydroxide, (c) sodium metasilicate, (d) glass fiber, (e) SH solution.

Table 1: Properties of granite soil samples.

Specific gravity d_s	Water content ω (%)	Density (g/m^3)	Liquid limit ω_l	Plastic limit ω_p
2.67	13	16.5	48.3	27

about 64% of silicon dioxide and 22.5% of sodium oxide, transparent after dissolving in water. Its relative molecular weight is 284.22.

SH polymer was a liquid-modified polyvinyl alcohol polymer with a 5% solute mass fraction in the original solution, from Lanzhou University, China [53]. SH polymer could be infinitely diluted with water, its density was 1.09 g/cm^3, and its relative molecular mass was about 2000. The solution shown in Figure 2(e) was the original SH polymer. As illustrated in Figure 2(d), the average length of the glass fiber used in the test was 12 mm. The glass fiber was an environmentally friendly inorganic nonmetallic material with excellent performance, which was used for the reinforcement of GRS in this experiment. The specific parameters of the glass fiber are shown in Table 2.

2.2. Preparation and Curing of Samples. The soil samples were baked in an oven for 7 h at about 105°C. The samples were removed from the oven after they dropped to room temperature, crushed, and sieved at 1.18 mm. The reinforcement materials were mixed with the soil samples evenly. A small compaction instrument was used to make the samples into a cylinder with a diameter of 100 mm and a height of 50 mm (Figure 3) by adding the soils three times. The samples were placed in a ventilated and dry indoor place and air-dried for 14 days. The sample weight is 1600 g.

2.3. Experimental Tests. The optimal water content test was carried out to investigate the optimal moisture content of the soil. The reinforced samples with optimal water content were subjected to a static load test and drop weight impact test, respectively. The reinforcement solutions containing different ratios of Si and Na were prepared under the optimal water content. Static load tests were applied to the samples with reinforcement solutions. Static load test plan 1 is given in Table 3. Different amounts of sodium hydroxide and sodium silicate were added to adjust the ratio of Si and Na in the samples (Table 3). Three samples were made for each ratio.

Table 2: Glass fiber parameters.

Density (g/cm^3)	Linear density (dtex)	Elastic modulus (MPa)	Tensile strength (MPa)	Melting point (°C)	Elongation (%)
0.91	8.21	4286	346	169	36.4

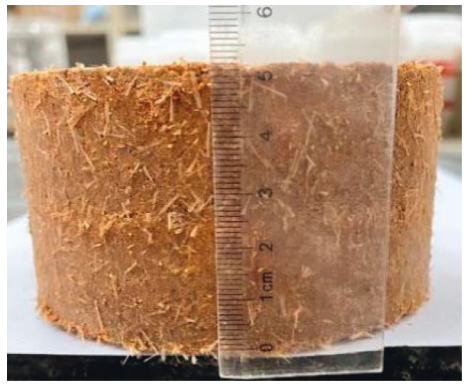

Figure 3: Reinforced soil sample.

Table 3: Static load test plan.

	Group	Si : Na	Water content (%)	Na_2SiO_3 (g)	NaOH (g)
Static load test	O	0	13	0	0
	A	1 : 1	13	40	5.80
	B	1 : 2	13	40	22.34
	C	1 : 3	13	40	40.0
	D	1 : 4	13	40	55.20
	E	1 : 5	13	40	71.68

The drop weight impact load test is given in Table 4. The optimal content of SH solutions is 3.5% and glass fibers 3%, both of which are formulated based on the mass of pure soil [42]. Therefore, the SH solution content is 3.5%, and glass fiber is 3% in this study. Group H was the control group, pure soil with a water content of 13%. Groups F and G were experimental groups. Group F consists of 3.5% SH solution and 3% glass fiber with a water content of 13% in addition to pure soil. Group G consists of Si : Na = 1 : 4 solutions and 3% glass fibers with a water content of 13% in addition to pure soil with a water content of 13%. Three samples were made for each condition. The word "LIT" represents samples with drop weight tests, "01" the SH solutions, "02" Si : Na = 1 : 4 solutions, and "00" pure soils. For example, LIT00 refers to pure soil samples.

2.4. Methods. The samples were prepared with seven water percentages (11%, 12%, 13%, 14%, 15%, 16%, 17%, and 18%) and compacted by a light compactor, after which the quality and water content of the samples were measured. The optimal water content curve raging within the range of 11–18% is given.

In the static load test, the uniaxial compressive strength of the sample was measured with a 4 W uniaxial nonlateral compressive tester (Figure 4). Specifically, the specimen was placed in the center of the plate to ensure that no eccentric loads occurred. The loading rate was 0.5 MPa/s. The loading axial force when the sample failed was recorded to calculate the uniaxial compressive strength of each sample with the following formula:

$$R = \frac{P}{A}. \tag{1}$$

R is the ultimate compressive strength of the sample, P is the maximum load when the sample failed, and A is the cross-sectional area of the sample.

The strength of the three samples under the same concentration was recorded. The strength values were averaged following the principle that the limit load does not exceed 10%. A static load test was used to obtain the best silicon-sodium ratio by measuring the compressive strength of samples under different ratios.

The Instron Ceast9350 floor drop weight impact tester for the dynamic impact load test is shown in Figure 5 [54]. The mass of the dropping weight was 3.065 kg. The load weight in the impact load test was 36.674 kg. The falling rate of the weight was 4.5 m/s, and the corresponding instantaneous impact energy was 403.13 J. The impact load on the sample was recorded by the pressure sensor on the drop weight. The compression was the displacement the drop weight had after touching the sample [54].

Table 4: Drop weight test plan.

	Group	Specimen number	SH solution (%)	Si : Na solution	Glass fiber (%)	Water content (%)
Drop weight test	F	LIT01	3.5	0	3	13
	G	LIT02	0	1 : 4	3	13
	H	LIT00	0	0	0	13

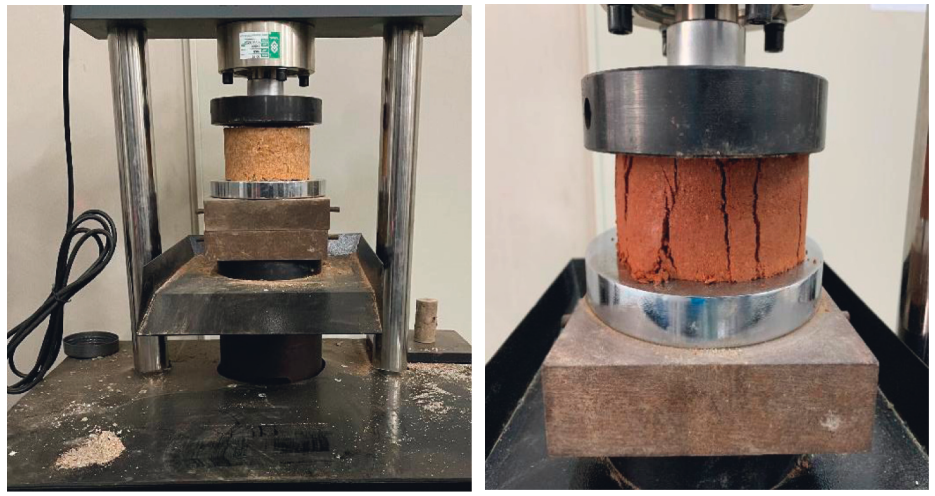

Figure 4: Uniaxial compression test instrument.

Figure 5: Drop weight tester.

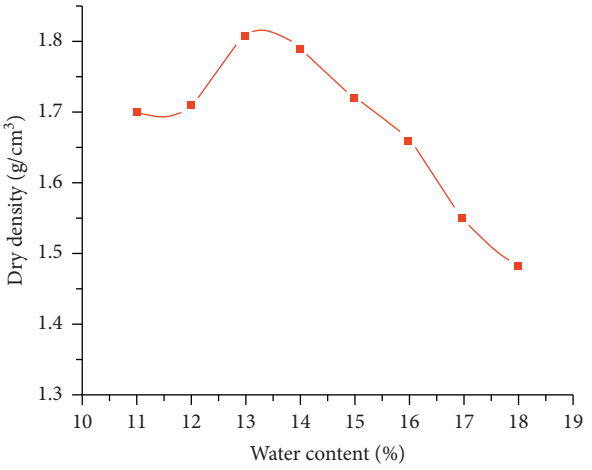

Figure 6: Optimal water content curve.

3. Results and Discussion

3.1. Optimal Water Content Test. The curve graph of the optimal water content and dry density from the compaction test is shown in Figure 6. Therefore, with the same amount of compaction, the dry density of the soil first increased with the rise of water content and topped at 1.81 g/cm^3 when the water content was 13% and decreased with the rise water content after that.

3.2. Static Load Test. In the static load test, the compressive strength of the reinforced samples is found to be 780 kPa, 1250 kPa, 4250 kPa, 4550 kPa, and 1600 kPa for incorporation of solution with a Si/Na ratio of 1 : 1, 1 : 2, 1 : 3, 1 : 4, and 1 : 5 (Groups A, B, C, D, and E), respectively, and 800 kPa for Control Group O. The stress-strain curve of each group with different silicon-to-sodium ratios is depicted in Figure 7. The result signifies that different silicon-sodium ratios have different reinforcement effects on soils, and the effect was remarkable at the optimal ratio (1 : 4). From Figure 7, a considerable rise in strength is witnessed with the decrease of the Si/Na ratio from 1 : 1 to 1 : 4. The strength at the ratios of 1 : 3 and 1 : 4 was about 300% higher than that of 1 : 1 and 1 : 2. However, when the Si/Na ratio decreases to 1 : 5, the strength dropped back to 1600 kPa, so the strength of the soil is not directly proportional to the ratio. Only in a certain range can the soil be strengthened and reinforced remarkably. Thus, the

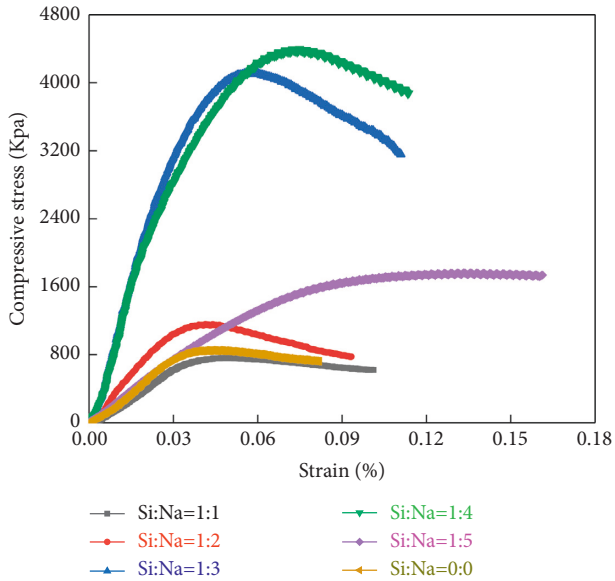

Figure 7: Compressive strength curve.

Si/Na ratio of 0.25 is the most economical choice for reinforcement regarding strength and deformation.

3.3. Drop Weight Test. The drop weight test can evaluate the ability of the sample to resist impact load. The dynamic response of the sample can be reflected by analyzing the instantaneous impact load of the falling weight, the compression of the sample, and the response time.

3.3.1. Impact Load Analysis. Results of the impact test with an initial velocity of 4.5 m/s (initial energy of 403.13 J) show that the SH solutions and the Si : Na = 1 : 4 solutions both can improve samples' ultimate bearing capacity as given in Figure 8. The ultimate bearing capacity of the undisturbed soil sample (LIT00) was 17.6 kN. That of SH solutions reinforced sample (LIT01) was 19.8 kN, 12.5% more than LIT00. The ultimate bearing capacity of Si : Na = 1 : 4 solutions sample (LIT02) was 98.5 kN, 459% and 397% higher than LIT00 and LIT01, respectively. In terms of deformation, the final deformation of LIT01 and LIT00 was quite similar, close to 38 mm, while that of LIT02 was only 17 mm. The deformation of LIT02 was 55.3% lower than that of LIT00 and LIT01, nearly half. It follows that glass fibers with Si : Na = 1 : 4 solutions can reinforce soil better than SH solutions, strengthen the soil, and reduce deformation significantly.

The effect of drop weight on the two samples reinforced with glass fibers under different solutions is given in Figure 9. The relationship between impact force and deformation is that the latter increases with the rise of the former in each test and vice versa. The impact load compressed the pores of GRS and forced soil grains to rearrange. These impact force-compression deformation curves can be divided into four stages: rearrangement, strengthening, peak, and weakening stage. This is consistent with the conclusions of Yuan et al. [42].

The peak impact load of the Control Group H (LIT00) stood at 17.6 kN, smaller than the experimental groups: Groups G and H. Both the Si : Na = 1 : 4 solutions and the SH solutions can significantly improve the impact load resistance of the samples. Although LIT01 and LIT02 were treated with different reinforcement solutions, their impact force-time travel curves are similar, as shown in Figure 8 that both curves have four stages. The impact load of LIT01 went straight up rapidly with the deformation range 0–3 mm, reached the first peak load, and then went downward. After hitting the first lower point, it climbed again, finally reached the ultimate load peak with about 30 mm deformation, and then dropped to 0 over with the final deformation of 38 mm. The impact load of LIT02 also went straight up rapidly with the deformation range 0–3 mm, reached the first peak load, and then went downward. After hitting the first lower point, it climbed again, finally reached the ultimate load peak with about 10 mm deformation, and then dropped to 0 over with the final deformation of 17 mm.

In the early stage, the impact load of the two shot up because elastic deformation happened in a short time under the impact speed of 4.5 m/s. At this moment, the external force disturbed soil granules and made them move and tumble, whereafter granules rearranged and aggregated. Pores became smaller, and the effective stress between particles increased, leading to a higher impact load. After the first peak, the impact force of the two samples began to decrease. Through analysis, the reason is that sample began to crack after the elastic deformation reached the maximum and aggravated the compression, thus resulting in a gradual reduction of impact load. The impact load rebound at about 4 mm deformation and then rose to the maximum peak. This is because the soil was compacted and its deformation modulus increased after it cracked to a certain extent. Meanwhile, the mixture of glass fibers and soil jointly bore the impact load of the falling weight, so the sample can be further compressed without being destroyed, which has been proved in Dey's study [55, 56].

In the increase phase and peak phase, the reinforcement effects of the two solutions are particularly different. For LIT01, although the impact force increased gradually, its deformation rose significantly and deformed 30 mm at the maximum impact force, while LIT02 deformed 10 mm at the maximum impact force, over 50% less than LIT01. The reason is that an adhesive substance similar to geopolymer was produced between soil particles under the Si : Na = 1 : 4 solutions. The substance can better bind the soil particles together into a whole with higher strength. By contrast, the SH solution is significantly inferior to the Si : Na = 1 : 4 solution in terms of viscosity.

3.3.2. Analysis of Compression and Test Response Time. The sample was compressed under the impact load. The time history curve of the displacement from compression is given in Figure 10. The compression displacement of the Control Group H (LIT00) is proportional to the time, and the slope of the curve is approximately equal to 4.5 m/s. The sample failed when the weight hit the sample with a speed of 4.5 m/s.

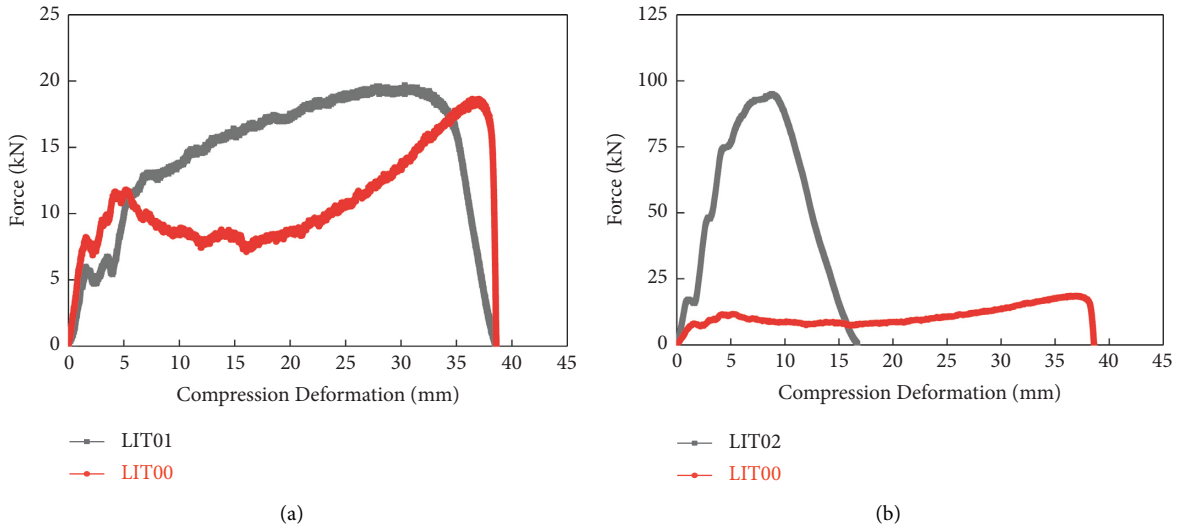

Figure 8: Diagram of impact force and compression deformation of specimen. (a) Groups F and H. (b) Groups G and H.

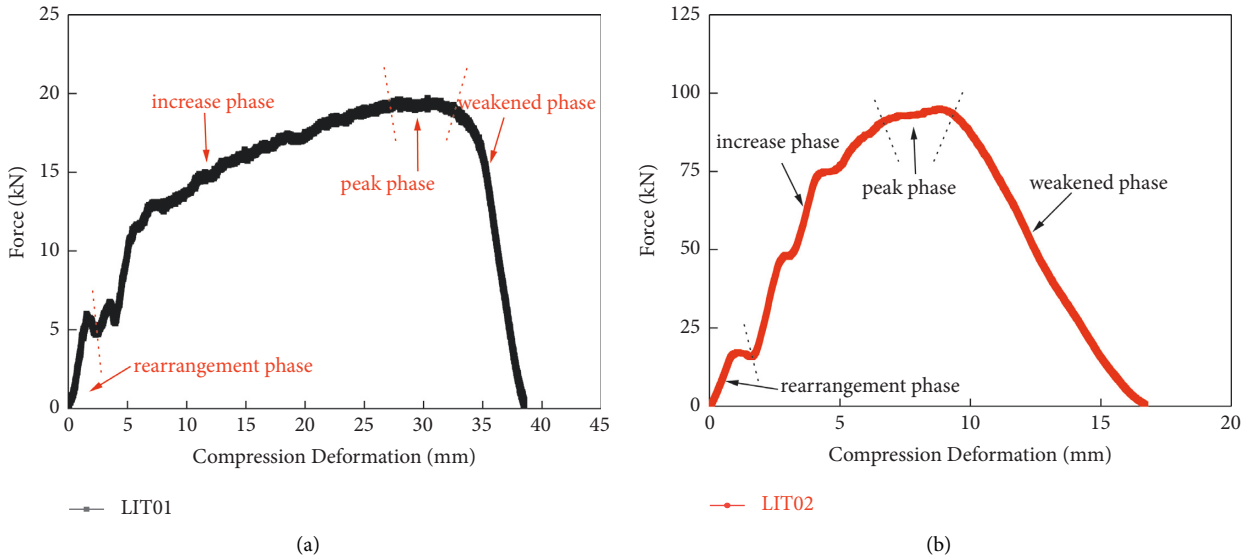

Figure 9: Diagram of impact force and compression deformation of specimen. (a) Group F. (b) Group G.

The force that acted on the weight was little, so the slope of the displacement compression curve is 4.5. It can be seen from Figure 10 that, under the impact load of drop weight, the compression of Group F (LIT01) and Group G (LIT02) in the initial stage first increased linearly with time and then nonlinearly to the maximum. The amount of compression fell after the peak, indicating that the sample had a certain degree of elastic spring back in the later loading stage. In sample LIT02, the maximum compression was 10 mm. Due to the elastic rebound of the soil, the final compression was 6 mm, and the response time 4.5 ms. In sample LIT01, the maximum compression amount was 29.8 mm. Due to the elastic rebound of the soil, the final compression amount was 28.6 mm, and the response time 14.8 ms. Thus, the compression amount and response time of LIT02 under impact load are minimum. This means when the glass fiber content is maintained at 3.0%, the Si : Na = 1 : 4 solutions have a much stronger effect on GRS than the SH solution, so it can be concluded that the reinforcement effect of Si : Na = 1 : 4 solution is better than the SH solution. Furthermore, SEM and XRD techniques can offer a microscopic perspective to analyze the influence of the two solutions on the mechanical properties of soil samples with glass fibers.

3.4. Scanning Electron Microscopy (SEM). Figure 11 shows images under SEM of some samples in Groups F, G, and H after being subjected to a drop weight test. As shown in the picture, at the magnification of 300x, the soil of the control Group H was granular particles with weak particle connections. As a consequence, the sample could not withstand the impact energy during shock loading and failed [57].

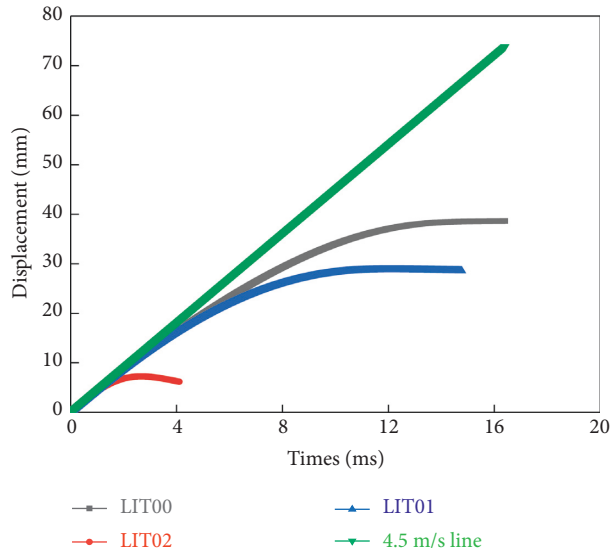

Figure 10: Compression amount time history curve.

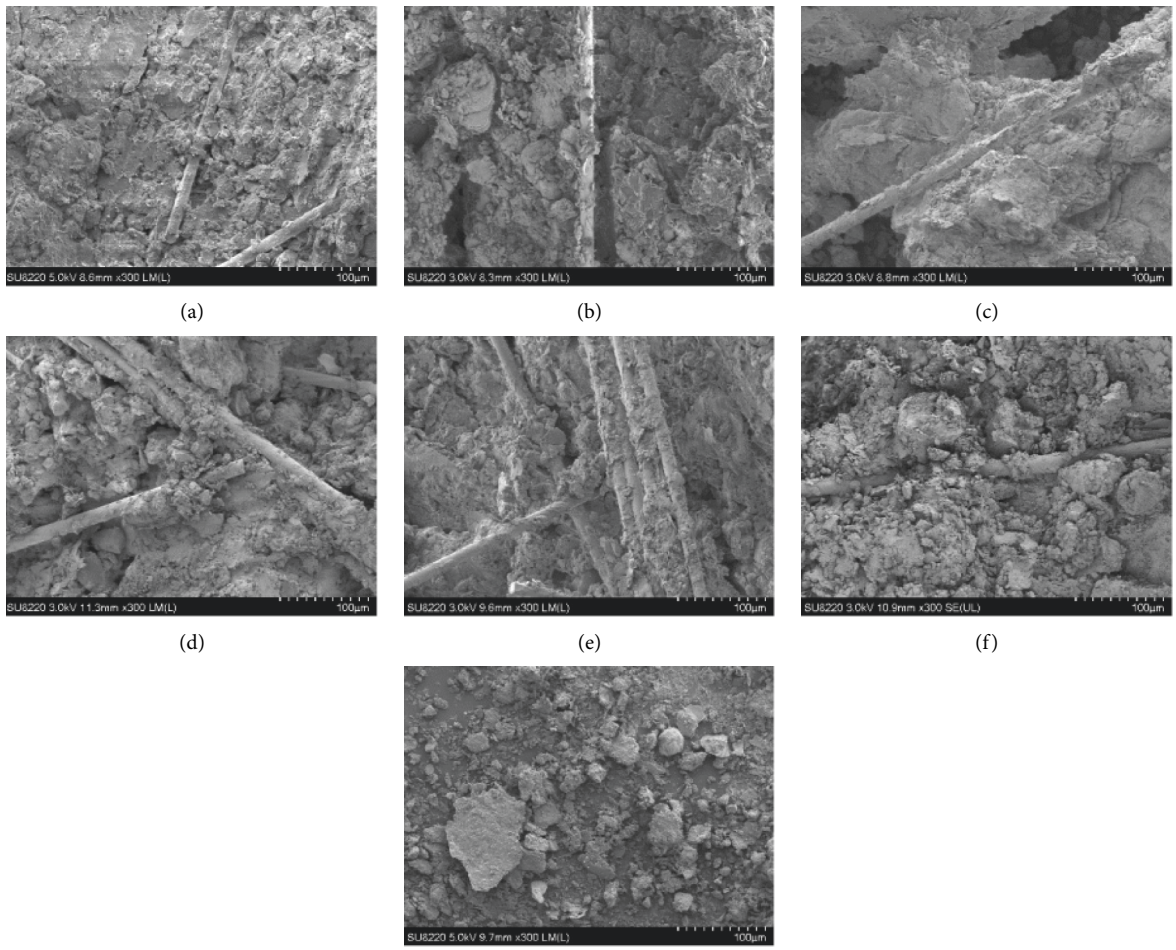

(a) (b) (c) (d) (e) (f) (g)

Figure 11: SEM of test soil magnification: 300. (a) F1. (b) F2. (c) F3. (d) G1. (e) G2. (f) G3. (g) H.

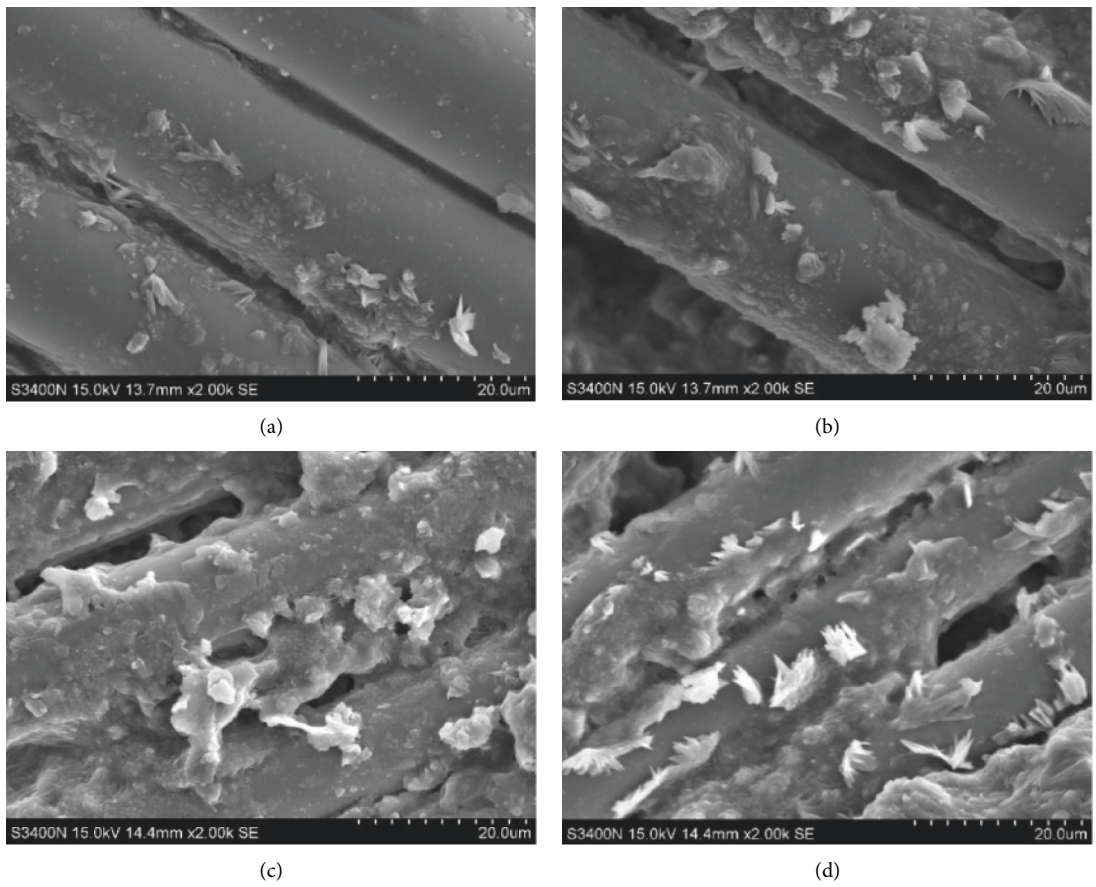

Figure 12: SEM of Group F and Group G magnification: 2000. (a) F1. (b) F2. (c) G1. (d) G2.

Compared with the SEM results of Group H, the soils of Groups F and G were more integral after impact load since the glass fiber bonded the soil together into an integral structure and jointly bore the external shock load. Glass fiber is the reinforcer in the soil, which increases the connection between particles and fibers, increases the friction force between them, improves the integrity of the soil, and thus improves the ultimate bearing capacity of the soil [58–61].

Figure 12 shows 2000x magnified images under SEM, which were taken at the junction of glass fiber and soil. Thus, less soil is attached to the glass fiber under the SH solution than under Si : Na = 1 : 4 solution. The glass fiber and the soil formed an interactive structure under Si : Na = 1 : 4 solutions. In the test, the load could be transferred from soil to fiber owing to its high tensile performance. The fiber shares part of the load; hence the overall impact resistance of the sample is improved. By contrast, glass fibers could not bond soil under SH solution as they did under Si : Na = 1 : 4 solution. Therefore, the connection between glass fibers and soil differs between the two solutions, which leads to a difference in the effective stress between soil particles and fibers. Si : Na = 1 : 4 solutions perform better than SH solutions in terms of reinforcing soil with glass fibers. This conclusion is proved by the drop weight test and confirmed by SEM.

3.5. XRD. XRD spectra (Figures 13 and 14) were obtained from test residues of LIT00, LIT01, and LIT02. The solid phase of GRS, reinforcement solutions, and glass fibers all changed during mechanical mixing. According to the powder diffraction file, the XRD pattern indicates that the main mineral components in LIT00 are kaolinite (as high as 67.8%), quartz, as well as a small amount of illite, and sodium-potassium feldspar. In LIT01, the diffraction strength and angle of quartz's characteristic diffraction peak (101) did not change markedly compared to LIT00, indicating that the quartz remained intact during mechanical mixing due to its high chemical stability [62]. Kaolinite, on the other hand, had three main reflections, with the strongest reflection at 12.3°. Compared to the XRD chart of LIT00, although their diffraction angle remained the same, the diffraction intensity fell significantly, indicating a decrease in the crystallinity of kaolinite and a lower kaolinite content. The most likely reason for this is that kaolinite particles bond with polymer SH, which lowers the crystallinity of the kaolinite. Microscopically, soil particles became more "integrated" and therefore more difficult to destroy when resisting shock loads [63].

In LIT02, the diffraction angle of quartz's characteristic diffraction peak was quite the same as in LIT00, as shown in Figure 14, and the quartz also maintains integral. However, the diffraction strength reduced remarkably, indicating that

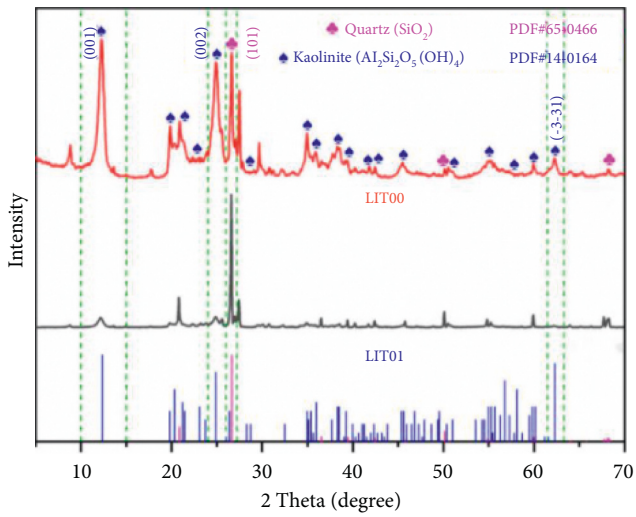

Figure 13: XRD patterns of LIT00 and LIT01.

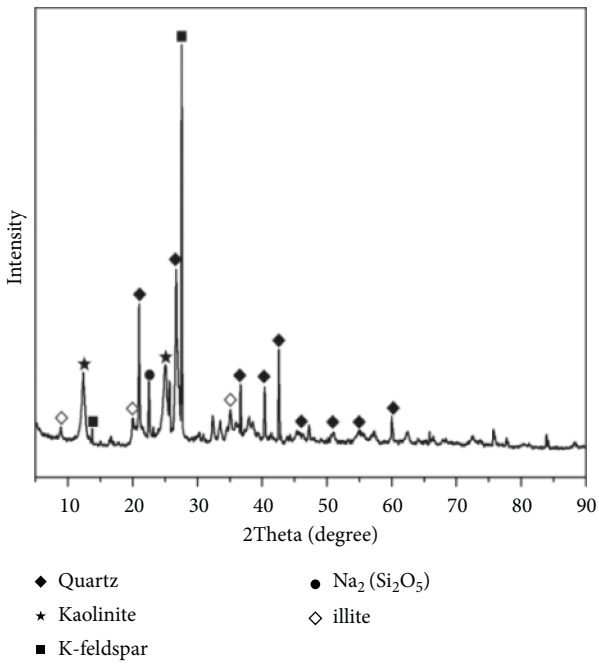

Figure 14: XRD patterns of LIT02.

the crystallinity of quartz and its content reduced. The most likely reason is that the kaolin particles react with a 1 : 4 sodium silicate solution, which affects the stability of quartz during decomposition and repolymerization. At the same time, potassium feldspar changes significantly after adding 1 : 4 sodium silicate solution, and the content of potassium feldspar increases significantly when the reflection angle is 27.8°. The added 1 : 4 sodium silicate solution may interact with potassium feldspar [64]. Potassium feldspar belongs to the monoclinic crystal system, whose main components are alumina, silicon dioxide, and potassium oxide. It is characterized by high stability, high strength, and excellent compressive performance. Most substances in LIT02 are quartz and potassium feldspar, both of which are stable. A small number of geopolymers and alkali-activated materials were formed in LIT02 after adding 1 : 4 sodium silicate solution [65, 66], and the generated geopolymers and alkali-activated materials had higher viscosity and strength. It fills in the pores of particles and adheres to them more firmly, which enhances the effective stress greatly and thus strengthens the soil [67]. Geopolymer bonds soil particles better with fibers into a whole load of the structure, which echoes the analysis in SEM. Therefore, the overall structure of the soil is stronger and more stable than LIT01, so it enjoys a higher bearing capacity.

Analyzed from a microscopic perspective, more substances with higher strength and stability were generated after adding Si : Na = 1 : 4 solutions and glass fibers. Soil particles were wrapped by the viscous geopolymer and aggregated as a whole structure with higher compressive strength and stability. In conclusion, based on microscopic analysis, the reinforcement effect of glass fibers under Si : Na = 1 : 4 solutions is significantly better than that of SH solutions.

4. Conclusions

GRS samples were subjected to static load tests and drop weight impact load tests with a control group. This study analyzed the influence of silicon-sodium ratios on GRS, discussed glass fibers' influence on the mechanical properties of GRS under different reinforcement solutions, and investigated the microscopic mechanism behind it. The main conclusions can be drawn below:

(1) The static load test shows that the sample exhibited the highest compressive strength of 4550 kPa with Si : Na = 1 : 4 solutions, significantly higher than pure soil samples. The ultimate compressive strength fell to 180 Mpa when the ratio went down, so the best reinforcement solution should be the one with silicon and sodium at the ratio of 1 : 4.

(2) The drop weight impact test shows that the glass fiber had the best reinforcement effect on GRS when its content was maintained at 3.0 under Si : Na = 1 : 4 solutions, which performed far better than SH solutions. The ultimate impact load of samples with Si : Na = 1 : 4 solutions was 98.5 kN, the response time was 4.5 ms, and the final compression was 6 mm. By contrast, the ultimate impact load of samples with SH solutions was 19.8 kN, the response time 14.8 ms and the final compression 28.6 mm.

(3) SEM and XRD analysis show that glass fibers can significantly improve samples' strength because of their high tensile strength. Glass fibers bound together with soil granules and formed an integral structure, jointly bearing the external load, thereby improving the strength. The Si : Na = 1 : 4 solutions are superior to the SH solutions because a kind of adhesive and high-strength geopolymer was produced under the Si : Na = 1 : 4 solutions. The geopolymer and alkali-activated materials clump the soil particles together more tightly. In addition, some

substances with stable chemical properties and high strength including potassium feldspar were also formed. With these substances binding the soil tightly, the effective stress between soil granules was enhanced, so the soil was reinforced with higher bearing capacity and stability. Geopolymers and alkali-activated materials are green and environmentally friendly materials, in line with the concept of sustainable development, and can provide a possibility for improving granite residual soil.

Data Availability

If necessary, data can be obtained from the corresponding author.

Conflicts of Interest

The authors declare that they have no conflicts of interest in this work.

Acknowledgments

The authors would like to gratefully acknowledge the support provided by the National Natural Science Foundation of China (nos. 51978177, 41902288, and 12072079). The editorial help from Professor Galen Leonhardy of Black Hawk College is also greatly appreciated. In addition, Taishan Fiberglass Inc. which provides glass fiber for experiments in this paper is also worthy of appreciation.

References

[1] S. Nanda and F. Berruti, "Municipal solid waste management and landfilling technologies: a review," *Environmental Chemistry Letters*, vol. 19, no. 2, pp. 1433–1456, 2020.

[2] A. S. Mohammed, "Material characterization of palm oil fuel ash (POFA) mixed with granite residual soil," *Advanced Materials Research*, vol. 955, pp. 2093–2097, 2014.

[3] A. Zhou, W. Zhang, and H. Wei, "A novel approach for recycling engineering sediment waste as sustainable supplementary cementitious materials," *Resources, Conservation and Recycling*, vol. 167, no. 12, Article ID 105435, 2021.

[4] J. Xiao, Z. Xu, Y. Murong et al., "effect of chemical composition of fine aggregate on the frictional behavior of concrete–soil interface under sulfuric acid environment," *Fractal and Fractional*, vol. 6, no. 1, 2022.

[5] Q. Wang, D. Tang, and Q. Zhang, "A study on the structure and composition of granite residual soil in the eastern China," *Journal of Changchun University of Earth Science*, vol. 1, pp. 73–81, 1991.

[6] H. Mei, X. Jian, W. Zhang, and H. S. Fu, "Behavioral differences between weathering and pedogenesis in a subtropical humid granitic terrain: implications for chemical weathering intensity evaluation," *Catena*, vol. 203, Article ID 105368, 2021.

[7] Y. Deng, X. Duan, S. Ding, and C. J. Cai, "Suction stress characteristics in granite red soils and their relationship with the collapsing gully in south China," *Catena*, vol. 171, pp. 505–522, 2018.

[8] B. Yuan, M. Sun, L. Xiong, and Q. Luo, "Investigation of 3D deformation of transparent soil around a laterally loaded pile based on a hydraulic gradient model test," *Journal of Building Engineering*, vol. 28, no. 6, Article ID 101024, 2020.

[9] X. Liu, X. Zhang, L. Kong, and G. H. Wang, "Formation mechanism of collapsing gully in southern China and the relationship with granite residual soil: a geotechnical perspective," *Catena*, vol. 210, Article ID 105890, 2022.

[10] J. Xia, C. Cai, Y. Wei, and X. Wu, "Granite residual soil properties in collapsing gullies of south China: spatial variations and effects on collapsing gully erosion," *Catena*, vol. 174, pp. 469–477, 2019.

[11] W. Jian, H. Hu, and Y. Luo, "Experimental study on deterioration of granite residual soil strength in wetting-drying cycles," *Journal of Engineering Geology*, vol. 25, no. 3, pp. 592–597, 2017.

[12] R. An, L. Hong, and C. Li, "Strength attenuation and microstructure damage of granite residual soils under hot and rainy weather," *Chinese Journal of Rock Mechanics and Engineering*, vol. 39, no. 4, pp. 743–751, 2017.

[13] C. Sun, *Research on Granite Residual Soil Engineering Properties and Subway Deep Foundation Pit Design Technology*, China University of Geosciences, Wuhan, China, 2014.

[14] W. Jian, W. Chen, and D. Zheng, "Experimental study on disintegration of granite residual soil," in *Proceedings of the Proceedings of the 9th Soil Mechanics and Geotechnical Engineering Conference of China Civil Engineering Society Beijing*, Architecture and Architecture Press, Hudson, New York, August 2003.

[15] Z. Nalbantoğlu, "Effectiveness of Class C fly ash as an expansive soil stabilizer," *Construction and Building Materials*, vol. 18, no. 6, pp. 377–381, 2004.

[16] P. Ghadir and N. Ranjbar, "Clayey soil stabilization using geopolymer and Portland cement," *Construction and Building Materials*, vol. 188, pp. 361–371, 2018.

[17] J. Xiao, J. Shen, M. Bai, and Q. Y. Gao, "Reuse of construction spoil in China: c," *Journal of Cleaner Production*, vol. 290, Article ID 125742, 2021.

[18] Q. Dong, G. Wang, X. Chen, and J. X. Tan, "Recycling of steel slag aggregate in portland cement concrete: an overview," *Journal of Cleaner Production*, vol. 282, Article ID 124447, 2021.

[19] B. Yuan, M. Sun, Y. Wang, and L. Zhai, "Full 3D displacement measuring system for 3D displacement field of soil around a laterally loaded pile in transparent soil," *International Journal of Geomechanics*, vol. 19, no. 5, pp. 1943–5622, 2019.

[20] R. Muduli and B. B. Mukharjee, "Effect of incorporation of metakaolin and recycled coarse aggregate on properties of concrete," *Journal of Cleaner Production*, vol. 209, pp. 398–414, 2019.

[21] B. Yuan, Z. Li, Z. Su, and Q. M. Z. Luo, "Sensitivity of multistage fill slope based on finite element model," *Advances in Civil Engineering*, vol. 2021, p. 13, 2021.

[22] J. Xiao, X. Long, W. Qu, and L. H. Z. Li, "Influence of sulfuric acid corrosion on concrete stress-strain relationship under uniaxial compression," *Measurement*, vol. 187, Article ID 110318, 2022.

[23] W. Liu, G. Ouyang, X. Luo, and J. L. M. Luo, "Moisture content, pore-water pressure and wetting front in granite residual soil during collapsing erosion with varying slope angle," *Geomorphology*, vol. 362, Article ID 107210, 2020.

[24] L. Zhao, *Study on Strength and Disintegration Characteristic of Improved Granite Eluvial Soil*, Hunan University of Science and Technology, Xiangtan, China, 2015.

[25] Y. Yao, J. Ni, and J. Li, "Stress-dependent water retention of granite residual soil and its implications for ground

settlement," *Computers and Geotechnics*, vol. 129, Article ID 103835, 2021.

[26] B. Yuan, L. Xiong, L. Zhai et al., "Transparent synthetic soil and its application in modeling of soil-structure interaction using optical system," *Frontiers of Earth Science*, vol. 7, 2019.

[27] Y. Wu, J. Cui, J. Huang, and W. N. L. Zhang, "Correlation of critical state strength properties with particle shape and surface fractal dimension of clinker ash," *International Journal of Geomechanics*, vol. 21, no. 6, Article ID 04021071, 2021.

[28] B. Zhang, H. Guo, P. Yuan, and Y. Q. L. D. Li, "Geopolymerization of halloysite via alkali-activation: d," *Applied Clay Science*, vol. 185, no. C, Article ID 105375, 2020.

[29] M. Kun, C. Chunyi, L. Zhimeng, H. Li, and H. Pei, "A new approach for longitudinal vibration of a large-diameter floating pipe pile in visco-elastic soil considering the three-dimensional wave effects," *Computers and Geotechnics*, vol. 128, Article ID 103840, 2020.

[30] B. Bai, Q. Nie, Y. Zhang, and X. W. Wang, "Cotransport of heavy metals and SiO2 particles at different temperatures by seepage," *Journal of Hydrology*, vol. 597, Article ID 125771, 2021.

[31] B. Yuan, Z. Li, Z. Zhao, H. Z. Ni, and Z. Li, "Experimental study of displacement field of layered soils surrounding laterally loaded pile based on transparent soil," *Journal of Soils and Sediments*, vol. 21, no. 9, pp. 3072–3083, 2021.

[32] X. Que, Z. Zhu, and W. Lu, "Anisotropic constitutive model of pentagonal prism columnar jointed rock mass," *Bulletin of Engineering Geology and the Environment*, vol. 79, no. 1, pp. 269–286, 2020.

[33] B. Bai, G.-C Yang, T. Li, and G.-s. Yang, "A thermodynamic constitutive model with temperature effect based on particle rearrangement for geomaterials," *Mechanics of Materials*, vol. 139, Article ID 103180, 2019.

[34] X. Que, Z. Zhu, Z. Niu, and W. Lu, "Estimating the strength and deformation of columnar jointed rock mass based on physical model test," *Bulletin of Engineering Geology and the Environment*, vol. 80, no. 2, pp. 1557–1570, 2020.

[35] W. Chen, Z. Li, J. Zhao, J. Lv, J. Song, and X. Cao, "Influence of groundwater depth on pile-soil mechanical properties and fractal characteristics under cyclic loading," *Fractal and Fractional*, vol. 6, no. 4, p. 198, 2022.

[36] Y. He, F. Gu, C. Xu, and Y. Wang, "Assessing of the influence of organic and inorganic amendments on the physical-chemical properties of a red soil (Ultisol) quality," *Catena*, vol. 183, Article ID 104231, 2019.

[37] Y.-H. Xie, C.-S. Tang, and B. Liu, "Ater stability improvement of clayey soil based on microbial induced calcite precipitation," *W Journal of Zhejiang University (Engineering Science)*, vol. 53, no. 8, pp. 1438–1447, 2019.

[38] B. Bai, R. Zhou, G. Cai, and W. G. Hu, "Coupled thermo-hydro-mechanical mechanism in view of the soil particle rearrangement of granular thermodynamics," *Computers and Geotechnics*, vol. 137, no. 8, Article ID 104272, 2021.

[39] N. E. N'Guessan, E. Joussein, A. Courtin-Nomade, E. Paineau, and P. Fondanèche, "Role of cations on the dissolution mechanism of kaolinite in high alkaline media," *Applied Clay Science*, vol. 205, Article ID 106037, 2021.

[40] L. Wang, R. Luo, W. Zhang, M. JIN, and S. TANG, "Effects of Fineness and Content of Phosphorus Slag on Cement Hydration, Permeability, Pore Structure and Fractal Dimension of Concrete," *Fractals*, vol. 29, 2020.

[41] B. Yang, J. Liu, X. Zhao, and S. Zheng, "Evaporation and Cracks of Soda Soil Improved by Fly Ash from Recycled Materials," *Land Degradation & Development*, vol. 32, 2021.

[42] B. Yuan, Z. Li, Y. Chen, and H. Ni, "Mechanical and microstructural properties of recycling granite residual soil reinforced with glass fiber and liquid-modified polyvinyl alcohol polymer," *Chemosphere*, vol. 286, no. P1, Article ID 131652, 2022.

[43] L. Feng, W. Zheng, L. Li, W. Feng, and G. Ning, "Mechanical and fatigue performance of rubber concrete," *Construction and Building Materials*, vol. 47, pp. 711–719, 2013.

[44] L. Feng, G. Chen, L. Li, and Y. Guo, "Study of impact performance of rubber reinforced concrete," *Construction and Building Materials*, vol. 36, pp. 604–616, 2012.

[45] M. Mirzababaei, A. Arulrajah, A. Haque, and S. A. Nimbalkar, "Effect of fiber reinforcement on shear strength and void ratio of soft clay," *Geosynthetics International*, vol. 25, no. 4, pp. 471–480, 2018.

[46] W. Feng, F. Liu, F. Yang, and L. L. Li, "Experimental study on dynamic split tensile properties of rubber concrete," *Construction and Building Materials*, vol. 165, pp. 675–687, 2018.

[47] Y. Guo, J. Xie, J. Zhao, and K. Zuo, "Utilization of unprocessed steel slag as fine aggregate in normal- and high-strength concrete," *Construction and Building Materials*, vol. 204, pp. 41–49, 2019.

[48] Y.-C. Guo, S.-H. Xiao, J.-J. Zeng, and J.-Y. Su, "Behavior of concrete-filled FRP tube columns internally reinforced with FRP-steel composite bars under axial compression," *Construction and Building Materials*, vol. 315, Article ID 125714, 2022.

[49] Y.-C. Guo, Y.-Y. Ye, L. Guan-Lin, and J.-F. Lv, "Effective usage of high strength steel tubes: axial compressive behavior of hybrid FRP-concrete-steel solid columns," *Thin-Walled Structures*, vol. 154, Article ID 106796, 2020.

[50] F. Ding, X. Wu, P. Xiang, and Z. Yu, "New damage ratio strength criterion for concrete and lightweight aggregate concrete," *ACI Structural Journal*, vol. 118, no. 6, pp. 165–178, 2021.

[51] B. Yang, S. Du, X. Zhao, D. Tang, and C. Yang, "Decision making of curriculum attainment degree for engineering geology based on fuzzy set theory," *Advances in Civil Engineering*, vol. 2021, Article ID 1743778, 6 pages, 2021.

[52] L. Wang, X. Song, H. Yang et al., "Pore structural and fractal analysis of the effects of MgO reactivity and dosage on permeability and F-T resistance of concrete," *Fractal and Fractional*, vol. 6, no. 2, p. 113, 2022.

[53] Y. Wang, C. Yang, W. Chen, and W. F. Han, "Strength characteristics and mechanism OF loess solidified with new polymer material SH," *Chinese Journal of Rock Mechanics and Engineering*, vol. 14, pp. 2554–2559, 2005.

[54] ASTM-INTERNATIONAL ASTM-International, *Standard Test Method for Determination of the Impact Value (IV) of a Soil*, ASTMD, West Conshohocken, PA, USA, 2015.

[55] V. Dey, A. Bonakdar, and B. Mobasher, "Low-velocity flexural impact response of fiber-reinforced aerated concrete," *Cement and Concrete Composites*, vol. 49, pp. 100–110, 2014.

[56] N. Banthia, C. Yan, and K. Sakai, "Impact resistance of fiber reinforced concrete at subnorma temperatures," *Cement and Concrete Composites*, vol. 20, no. 5, pp. 393–404, 1998.

[57] L. Zeng, H.-b. Bian, Z.-n. Shi, and Z.-m. He, "Forming condition of transient saturated zone and its distribution in residual slope under rainfall conditions," *Journal of Central South University*, vol. 24, no. 8, pp. 1866–1880, 2017.

[58] D. Gupta and A. Kumar, "Strength characterization of cement stabilized and fiber reinforced clay-pond ash mixes," *International Journal of Geosynthetics and Ground Engineering*, vol. 2, no. 4, p. 32, 2016.

[59] E. Kapogianni, M. Sakellariou, J. Laue, and S. Springman, "Investigation of the mechanical behaviour of the interface between soil and reinforcement, via experimental and numerical modelling," *Procedia Engineering*, vol. 143, pp. 419–426, 2016.

[60] A. M. Namjoo, K. Jafari, and V. Toufigh, "Effect of particle size of sand and surface properties of reinforcement on sand-geosynthetics and sand-carbon fiber polymer interface shear behavior," *Transportation Geotechnics*, vol. 24, Article ID 100403, 2020.

[61] B. N. Madhusudhan, B. A. Baudet, P. M. V. Ferreira, and P. Sammonds, "Performance of fiber reinforcement in completely decomposed granite," *Journal of Geotechnical and Geoenvironmental Engineering*, vol. 143, no. 8, Article ID 04017038, 2017.

[62] B. Zhang, H. Guo, L. Deng, and W. T. Q. Fan, "Undehydrated kaolinite as materials for the preparation of geopolymer through phosphoric acid-activation," *Applied Clay Science*, vol. 199, Article ID 105887, 2020.

[63] M. Tămăşan, T. Radu, and V. Simon, "Spectroscopic characterisation and in vitro behaviour of kaolinite polyvinyl alcohol nanocomposite," *Applied Clay Science*, vol. 72, pp. 147–154, 2013.

[64] J. Jalali, M. Balghouthi, and H. Ezzaouia, "Characterization of porous clay ceramics used to remove salt from the saline soils," *Applied Clay Science*, vol. 126, pp. 259–267, 2016.

[65] L. Bouna, A. Ait El Fakir, A. Benlhachemi, and K. M. B. S. F. N. Draoui, "Synthesis and characterization of mesoporous geopolymer based on Moroccan kaolinite rich clay," *Applied Clay Science*, vol. 196, Article ID 105764, 2020.

[66] S. S. Rahman and M. J. Khattak, "Roller compacted geopolymer concrete using recycled concrete aggregate," *Construction and Building Materials*, vol. 283, Article ID 122624, 2021.

[67] H. Guo, B. Zhang, L. Deng, and P. M. Q. Yuan, "Preparation of high-performance silico-aluminophosphate geopolymers using fly ash and metakaolin as raw materials," *Applied Clay Science*, vol. 204, Article ID 106019, 2021.